## PAPER

# Carbon dioxide hydrogenation over the carbon-terminated niobium carbide (111) surface: a density functional theory study

Saeedeh Sarabadani Tafreshi, [ID] *[a] Mahkameh Ranjbar,[a] Maryam Jamaati,[b] S. F. K. S. Panahi, [ID] [b] Narges Taghizade, [ID] [b] Mostafa Torkashvand[a] and Nora H. de Leeuw [ID] *[cd]

Carbon dioxide ($CO_2$) hydrogenation is an energetic process which could be made more efficient through the use of effective catalysts, for example transition metal carbides. Here, we have employed calculations based on the density functional theory (DFT) to evaluate the reaction processes of $CO_2$ hydrogenation to methane ($CH_4$), carbon monoxide (CO), methanol ($CH_3OH$), formaldehyde ($CH_2O$), and formic acid (HCOOH) over the carbon-terminated niobium carbide (111) surface. First, we have studied the adsorption geometries and energies of 25 different surface-adsorbed species, followed by calculations of all of the elementary steps in the $CO_2$ hydrogenation process. The theoretical findings indicate that the NbC (111) surface has higher catalytic activity towards $CO_2$ methanation, releasing 4.902 eV in energy. CO represents the second-most preferred product, followed by $CH_3OH$, $CH_2O$, and HCOOH, all of which have exothermic reaction energies of 4.107, 2.435, 1.090, and 0.163 eV, respectively. Except for the mechanism that goes through HCOOH to produce $CH_2O$, all favourable hydrogenation reactions lead to desired compounds through the creation of the dihydroxycarbene (HOCOH) intermediate. Along these routes, $CH_3^*$ hydrogenation to $CH_4^*$ has the highest endothermic reaction energy of 3.105 eV, while CO production from HCO dehydrogenation causes the highest exothermic reaction energy of −3.049 eV. The surface-adsorbed $CO_2$ hydrogenation intermediates have minimal effect on the electronic structure and interact only weakly with the surface. Our results are consistent with experimental observations.

## 1. Introduction

Recent years have seen a significant increase in interest in the remarkable physical and chemical features of transition metal carbides (TMCs).[1,2] They are carbon-containing close-packed metals exhibiting a remarkable mix of properties, combining the good electric and thermal conductance of transition metals, coupled with the toughness and structural coordination of covalent solids, and the high melting temperatures of ionic solids.[3–5] TMCs have been proposed as viable alternatives for valuable metals as a result of their intrinsic advantages of abundance, high reactivity, endurance, and affordability. Owing to their three distinct types of bonding: metallic, ionic, and covalent they are promising materials for a broad spectrum of technical applications of economic value.[6,7] The discovery in a seminal study by Levy and Boudart[8] of platinum-like behaviour in TMCs equivalent to that of Pt-group metals attracted significant interest in their potential use in a broad variety of catalytic processes, *e.g.* the water–gas shift,[9–11] CO hydrogenation[12] and $CO_2$ hydrogenation[12–20] reactions.

Carbon dioxide is one of the Earth's most significant pollutants and a potent active greenhouse gas, and rising $CO_2$ levels have been linked to global warming and other negative effects on the environment.[13,19,21] As a result, substantial research has been conducted into the alleviation of its adverse effects and the transformation of $CO_2$ into useful products, particularly in the context of producing sustainable energy.[22–24] However, the stability of $CO_2$ and the high adsorption energy restricts the number of potential viable catalysts.[13,20,25] A high activation barrier in C–O bond breaking requires highly efficacious catalysts.

*[a] Department of Chemistry, Amirkabir University of Technology (Tehran Polytechnic), No. 350, Hafez Avenue, 1591634311 Tehran, Iran. E-mail: s.s.tafreshi@aut.ac.ir*

*[b] Department of Physics, Iran University of Science and Technology, Narmak, 16846-13114 Tehran, Iran*

*[c] School of Chemistry, University of Leeds, LT2 9JT Leeds, UK. E-mail: N.H.deLeeuw@leeds.ac.uk*

*[d] Department of Earth Sciences, Utrecht University, 3584 CB Utrecht, The Netherlands*

Previous studies have been carried out to gain insight into $CO_2$ adsorbtion and conversion into usable hydrocarbon alternatives at low-index TMC surfaces,[13,15,20,22] where niobium carbide has been shown to be a substantial generator of CO and the key product of $CH_4$.[15] As such, NbC has been the topic of a number of experiments to investigate and customise its various characteristics.[26,27] Two often-researched NbC crystalline surfaces are the (100) plane, containing both metal and carbon atoms, and the (111) surface, which is terminated by either metal or carbon atoms that alternate in each layer.[7] The (111) surface of NbC has been shown to be more active towards gas adsorption than the (100) surface, owing to the higher electronic density of states around the Fermi level at the (111) surface.[7,28–31]

Our previous study has investigated $CO_2$ hydrogenation at the niobium-terminated NbC (111) surface,[32] where we found that the most likely products are $CH_4$ and CO. In contrast to the carbon-terminated (111) surfaces of TMCs at the top of the TM group, like the TiC (111) surface which proved to be unstable,[33] the carbon-terminated NbC surface was found to be important in a number of studies.[5,7,20,34] However, although an experimental study on $CO_2$ hydrogenation at the NbC (111) surface has been carried out by Prosoff and coworkers,[15] who found that CO and $CH_4$ are the main products, theoretical investigations of these processes, providing further detail on the reaction mechanism and formed intermediates, are still lacking. In this work, we have therefore carried out a comprehensive computational investigation of the network of reactions involved in $CO_2$ hydrogenation at the carbon-terminated NbC (111) surface.

Identifying the mechanism of $CO_2$ hydrogenation and the energetics of the elementary steps is important if we are to gain a better understanding of the formation and scission of the bonds which can aid in the development of active catalysts for the conversion of $CO_2$ into methane ($CH_4$), carbon monoxide (CO), methanol ($CH_3OH$), formaldehyde ($CH_2O$), and formic acid (HCOOH) during the hydrogenation mechanism. We have used calculations based on the density functional theory (DFT) with periodic surface models to elucidate the $CO_2$ hydrogenation intermediates and elementary steps on the carbon-terminated NbC (111), where we have focused on the geometric and energetic properties of the adsorbed species, as well as an in-depth examination of the electronic characteristics of the $CO_2$ hydrogenation products on the C-terminated NbC (111) surface, which is critical for the development of more effective TMC catalysts. In agreement with experiment,[15] we found that $CH_4$ and CO are indeed the predominant products of $CO_2$ hydrogenation at the C-terminated NbC (111) surface.

## 2. Computational details

### Method

The Vienna *Ab Initio* Simulation Package (VASP)[35,36] has been used to perform the computations. The Perdew–Burke–Ernzerhof (PBE) variant of the extended gradient estimation within the projector augmented wave (PAW) approach has been used for the total energy calculations.[37–39] As recommended by Grimme, the DFT-D3[40] inclusion of the dispersion interactions was also taken into consideration in order to enhance the accuracy of the energy characterization of each system. Plane waves featuring a cut-off energy of 600 eV were used to extend the Kohn–Sham orbitals in the bulk and slab calculations. Monkhorst-Pack grids[41] with meshes of $11 \times 11 \times 11$ and $4 \times 4 \times 1$ points were used to sample the Brillouin domain of the bulk and NbC (111) surface, respectively. The remaining forces and energies were adjusted until they fell below $0.01$ eV $\text{Å}^{-1}$ and $10^{-5}$ eV, respectively. Interference between the simulation system and its images was avoided by creating a vacuum space larger than 20 Å between the surface slabs. DFT-D3 is the primary methodology used for these types of calculations in the field of heterogeneous catalysis, with similar set-ups having been reported widely in the literature, thus enabling direct comparison of our results with previous work.[32,42,43] Solvent effects were not included in our calculations. Although these may affect the adsorption characteristics of the various molecules at the surface, they would not alter significantly the relative energies of the adsorbed intermediates and thus would not affect the trends identified in this work.

### Model

The NbC (111) surface has a hexagonal close-packed (hcp) composition terminated by either Nb or carbon atoms, which comprise the alternating layers. Other than the carbon-terminated NbC (111) surface, previous investigations in the literature have shown that carbon-terminated TMC (111) surfaces were unsustainable.[5,7,20,34] Here, we have solely focused on the C-terminated NbC (111) surface, as this termination may play an essential role in the conversion of $CO_2$ (see Fig. 1a). The calculated lattice constant of $a_0 = 4.53$ Å is in excellent agreement with the results of previous numerical ($a_0 = 4.51, 4.488$ Å)[3] and empirical ($a_0 = 4.469$ Å)[44] studies. To model the surface, a supercell of 112 atoms was used, consisting of seven atomic layers, four of which were kept frozen at their bulk optimised positions to mimic the bulk material. To determine the most stable and favourable adsorption geometry, each adsorbate was initially put in numerous surface sites before full geometry optimisation. The adsorption energy of each adsorbate ($E_{ads}$) can be determined as follows:

$$E_{ads} = E_{A+slab} - E_A - E_{slab} \tag{1}$$

where $E_{A+slab}$, $E_A$, and $E_{slab}$ represent the total energies of, respectively, the system with relaxed adsorbates on the NbC (111) plane, the isolated adsorbates, and the bare NbC (111) slab. Additionally, using equation (2), changes in the charge densities have been determined as the difference between the charge density of the molecule + NbC (111) complex and the charge density of the separate molecule and surface entities in the same geometry as the complex:

$$\rho = \rho_{Molecule+NbC(111)} - \rho_{NbC(111)} - \rho_{Molecule} \tag{2}$$

This journal is © the Owner Societies 2023

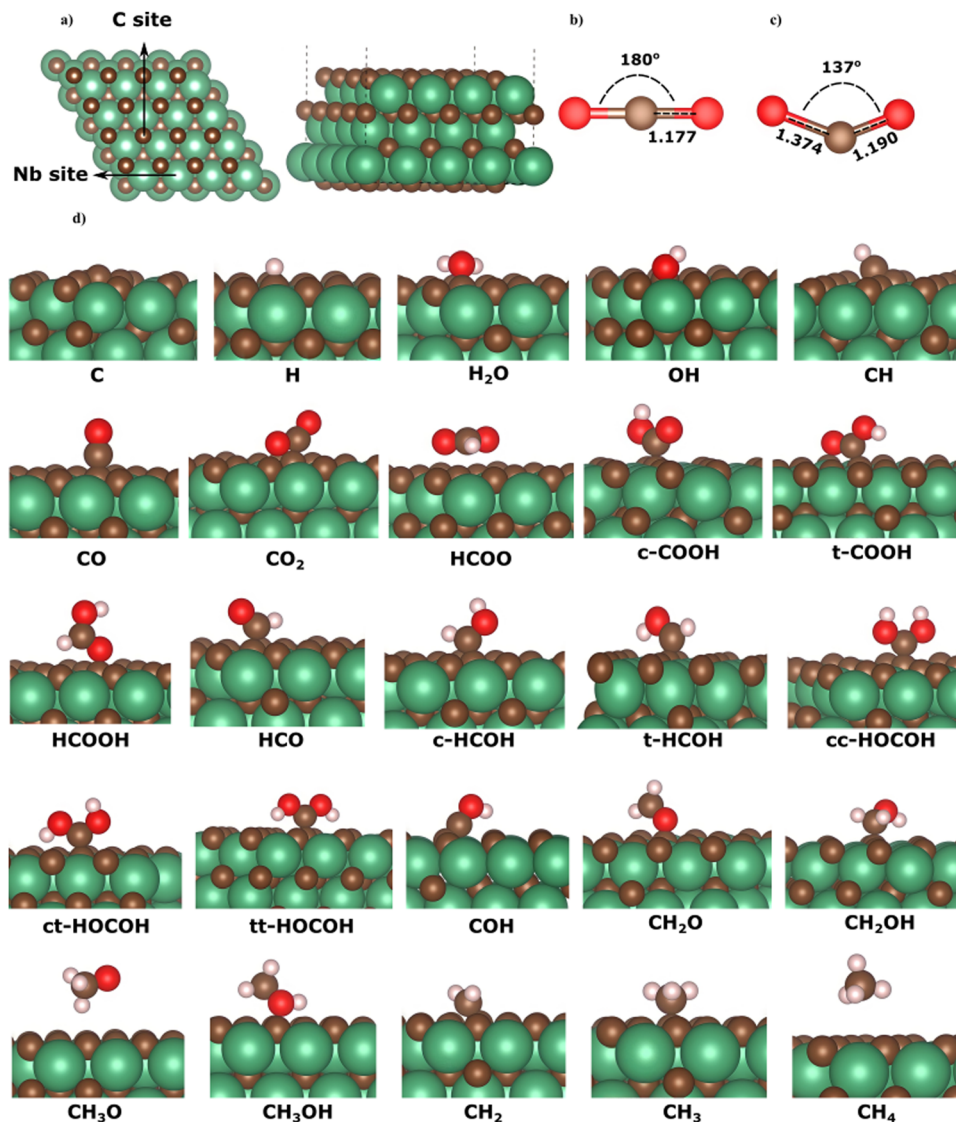*Phys. Chem. Chem. Phys.*, 2023, **25**, 2498–2509 | **2499**

Fig. 1 (a) The NbC (111) plane, and the isolated $CO_2$ molecule (b) prior to, and (c) following adsorption, and (d) adsorption structures with minimum energy for all intermediates on the NbC (111) plane.

where $\rho_{\text{Molecule+NbC(111)}}$, $\rho_{\text{NbC(111)}}$, and $\rho_{\text{Molecule}}$ are the overall charges of the relaxed molecule on the NbC (111) slab, the isolated NbC (111), and isolated molecule, respectively.

The methodology employed in this study has already been validated in previous studies reported in the literature.[32,45]

## 3. Results

### 3.1 Adsorption configurations and energies on NbC (111) plane

Here, we describe the adsorption on the C-terminated NbC (111) plane of all potential intermediates during the hydrogenation reactions of $CO_2$. Numerous preliminary configurations of the molecules situated above the NbC (111) plane at different positions were constructed. The most suitable adsorption site was selected following thorough structural optimization of

both the NbC (111) plane and the intermediates. Fig. 1 shows the geometries of the lowest energy adsorptions of all intermediates on the NbC (111) plane. Table 1 likewise provides geometry and energy data, where binding between the species and the surface is denoted by the * sign, whereas the chemical bonds in each intermediate following adsorption are depicted without markings.

$CO_2$. To evaluate the adsorption mechanism, we deposited $CO_2$ onto a relaxed NbC (111) slab. A C–C connection is formed between the $CO_2$ and the surface as it approaches a surface C atom. Furthermore, with a bond length of 1.62 Å, one of the oxygen atoms of the $CO_2$ binds to the surface C atom. As the C–O bond lengths change from 1.177 Å to 1.190 Å and 1.374 Å, the $CO_2$ adsorption leads to an alteration of its original arrangement, including a change to the O–C–O angle which reduces from 180° to 137°, which indicates activation of the $CO_2$ molecule on the surface. Fig. 1a–c shows the NbC (111)

**Table 1** Lowest energy adsorption data of all intermediate species within the $CO_2$ hydrogenation process at the NbC (111) plane. Intermediates–surface bonds are denoted by a * while chemical linkages within each intermediate following adsorption are indicated as unmarked

| Species | $E_{ads}$ (eV) | Bond length (Å) | Species | $E_{ads}$ (eV) | Bond length (Å) |
|---|---|---|---|---|---|
| H | −5.130, −3.52[45] | $d^\star_{H–C} = 1.10$ | $t$-HCOH | −6.342, −5.35[45] | $d^\star_{C–C} = 1.39$ $d_{O–C} = 1.31$ $d_{C–H} = 1.10$ $d_{O–H} = 1.00$ |
| C | −11.757 −7.61[45] | $d^\star_{C–C} = 1.35$ | $cc$-HOCOH | −4.824 | $d^\star_{C–C} = 1.39$ $d_{O–C} = 1.34$ $d_{O–H} = 0.98$ |
| $H_2O$ | −1.226, −0.997,[32] −1.33[10] | $d^\star_{C–O} = 1.48$ $d_{H–O} = 1.01$ $d_{H–O} = 1.04$ | $ct$-HOCOH | −5.302 | $d^\star_{C–C} = 1.40$ $d_{O–C} = 1.32$ $d_{O–H} = 0.98, 1.01$ |
| OH | −5.304, −5.52,[45] −5.427[32] | $d^\star_{C–O} = 1.31$ $d_{H–O} = 0.98$ | $tt$-HOCOH | −5.561 | $d^\star_{C–C} = 1.42$ $d_{O–C} = 1.31$ $d_{O–H} = 1.00$ |
| CH | −9.442, −7.29,[45] −7.404[32] | $d^\star_{C–C} = 1.22$ $d_{C–H} = 1.08$ | COH | −7.347, −4.88[45] | $d^\star_{C–C} = 1.26$ $d_{O–C} = 1.27$ $d_{O–H} = 1.01$ |
| CO | −4.008, −2.48[45] | $d^\star_{C–C} = 1.32$ $d_{O–C} = 1.17$ | $CH_2O$ | −1.908, −2.63[45] | $d^\star_{O–C} = 1.36$ $d_{O–C} = 1.28$ $d_{C–H} = 1.09$ |
| $CO_2$ | −0.358, −0.27[10] | $d^\star_{C–C} = 1.44$ $d^\star_{C–O} = 1.62$ $d_{O–C} = 1.19, 1.37$ | $CH_2OH$ | −4.219, −3.293,[32] −3.09[45] | $d^\star_{C–C} = 1.50$ $d_{O–C} = 1.40$ $d_{O–H} = 0.99$ $d_{C–H} = 1.11, 1.12$ |
| HCOO | −0.469, −5.222[32] | $d_{O–C} = 1.25$ $d_{C–H} = 1.17$ | $CH_3O$ | −0.261 | $d_{O–C} = 1.33$ $d_{C–H} = 1.13, 1.12$ |
| $c$-COOH | −4.155, −4.105[32] | $d^\star_{C–C} = 1.48$ $d_{O–C} = 1.22, 1.36$ $d_{O–H} = 0.98$ | $CH_3OH$ | −1.614, −0.72,[45] −0.959[32] | $d^\star_{O–C} = 1.46$ $d_{O–H} = 1.00$ $d_{O–C} = 1.49$ $d_{C–H} = 1.09$ |
| $t$-COOH | −4.408, −3.959[32] | $d^\star_{C–C} = 1.42$ $d_{O–C} = 1.27, 1.32$ $d_{O–H} = 0.98$ | $CH_2$ | −7.418, −5.797,[32] −5.81[45] | $d^\star_{C–C} = 1.36$ $d_{C–H} = 1.10$ |
| HCOOH | −1.539, −1.642[32] | $d^\star_{C–O} = 1.41$ $d_{O–C} = 1.28, 1.31$ $d_{O–H} = 0.98$ $d_{C–H} = 1.10$ | $CH_3$ | −4.528, −3.58,[45] −3.721[32] | $d^\star_{C–C} = 1.49$ $d_{H–C} = 1.10$ |
| HCO | −4.214, −3.74,[45] −4.240[32] | $d^\star_{C–C} = 1.48$ $d_{O–C} = 1.22$ $d_{C–H} = 1.11$ | $CH_4$ | −0.161, −0.298,[32] −0.17[45] | $d_{H–C} = 1.10$ |
| $c$-HCOH | −6.232 | $d^\star_{C–C} = 1.38$ $d_{O–C} = 1.33$ $d_{O–H} = 0.98$ $d_{C–H} = 1.10$ | | | |

slab and $CO_2$ prior to and following attachment. $CO_2$ hydrogenation on this plane is more likely than on the Nb-terminated plane, where the adsorption energy was large (−1.863 eV),[32] as shown by the calculated adsorption energy of −0.358 eV, which is in agreement with the results of the study by Liu *et al.* on the C-terminated $Mo_2C$ (001) surface with an adsorption energy of −0.27 eV for $CO_2$.[10] As such, the C-terminated NbC (111) could be an effective catalyst for $CO_2$ hydrogenation processes.

For each intermediate in the $CO_2$ hydrogenation reaction network, we have reported the geometries and energies of adsorption in the next section.

**C.** With an adsorption energy of −11.757 eV and a C–C bond length of 1.35 Å, C is strongly adsorbed on the NbC (111), in agreement with the study on the $Mo_2C$ (100) and $Mo_2C$ (110) surfaces where large adsorption energies of −7.61 and −7.71 eV, respectively, were obtained for the carbon atom.[45]

**H.** Hydrogen forms an H–C connection with a bond length of 1.10 Å to the NbC (111) surface, where it tends to adsorb directly on top of a surface C atom with an adsorption energy of −5.130 eV. This large adsorption energy is in line with the findings of Silveri *et al.*, who demonstrated that metal sites are less suitable for the attachment of the hydrogen atom.[34] The NbC surface, however, is more electron-rich than the TMCs containing smaller d orbitals, like TiC, with a narrower spatial expansion. As a result, it is more appealing for adsorption, and the adsorption energy is larger than TiC.[28] Large adsorption energies for H atoms at TMC surfaces were also seen in the work by Qi *et al.*, obtaining −3.52 and −3.26 eV for the $Mo_2C$ (100) and $Mo_2C$ (110) surfaces, respectively.[45]

**$H_2O$.** Water adsorbes with an energy of −1.226 eV, and it prefers to adsorb at a bridging site through its O atom (consistent with the literature[10]).

**OH.** The large adsorption energy of −5.304 eV is achieved when the molecule adsorbs at a bridging site, where its oxygen atom links to a carbon atom on the surface, in agreement with the literature.[10,45]

This journal is © the Owner Societies 2023

*Phys. Chem. Chem. Phys.*, 2023, **25**, 2498–2509 | **2501**

**CH.** With an adsorption energy of −9.442 eV, CH tends to adsorb virtually on top of a C atom on the NbC (111) surface at a bond distance of 1.22 Å. The large adsorption energy is in accord with CH adsorption on $Mo_2C$ surfaces (−7.29 and −7.11 eV).[45]

**CO.** CO attaches to the NbC (111) plane through its C atom sited on top of the carbon atom of the surface, with a C–C bond length and adsorption energy of 1.32 Å and −4.008 eV, respectively. During the adsorption phase, the C–O bond length increases by around 0.03 Å.

**HCOO.** This molecule binds to the bridging site, almost above an underlying Nb atom, with a short distance between the C atom of HCOO and the C atom of the NbC (111) plane of approximately 2.01 Å. The adsorption energy of HCOO is −0.469 and no chemical bond is formed.

**Cis-COOH and trans-COOH.** C–C bonds with lengths of 1.48 Å and 1.42 Å were formed, respectively, when these molecules approach the surface. The *c*-COOH attaches directly on top of a surface C atom, but the *t*-COOH is inclined toward the bridging site in such a manner that the O atom of the *t*-COOH interacts with the underlying Nb atoms. *c*-COOH and *t*-COOH have adsorption energies of −4.155 eV and −4.408 eV, respectively.

**HCOOH.** Adsorption occurs on top of a surface C atom through an O–C bond with a bond length of 1.41 Å, and an adsorption energy of −1.539 eV. Due to the adsorption, the C–O bond lengths in the HCOOH molecule change, one decreasing by 3.7% and the other increasing by 5.8%.

**HCO.** With a C–C bond length of 1.48 Å and adsorption energy of −4.214 eV, HCO attaches to the surface through a surface C atom of NbC (111), with the molecule slightly inclined to the bridging site.

**Cis-HCOH and trans-HCOH.** These molecules adsorb in such a manner that the C atoms of *c*-HCOH and *t*-HCOH form a C–C bond to a C atom of the NbC (111) surface, with bond lengths of 1.38 Å and 1.39 Å for the *cis* and *trans* conformers, respectively. With an adsorption energy of −6.342 eV, the *t*-HCOH is attached directly above the surface C atom, while the *c*-HCOH molecule shifts to the bridging site with an adsorption energy of −6.232 eV, in accord with the 5.35 eV released for these molecules on the molybdenum carbide surface.[45]

**Cc-HOCOH, ct-HOCOH and tt-HOCOH.** These dihydroxycarbene molecules are adsorbed on surface C atoms, with C–C bond lengths of 1.39 Å, 1.40 Å and 1.42 Å, and adsorption energies of −4.824 eV, −5.302 eV and −5.561 eV for *cc*-HOCOH, *ct*-HOCOH and *tt*-HOCOH, respectively.

**COH.** With an adsorption energy of −7.347 eV and a bond length of 1.26 Å, COH attaches to the surface through its C atom by forming a C–C bond.

**CH₂O.** This molecule attaches to a surface C atom through its O atom with a C–O bond length of 1.36 Å and adsorption energy of −1.908 eV.

**CH₂OH.** With an adsorption energy of −4.219 eV, this molecule attaches to a surface C site on NbC (111) *via* its C atom with a C–C bond length of 1.50 Å. Following adsorption, the original C–O bond length increases by 2.9%.

**CH₃O.** CH₃O adsorbs to the surface through its H atom, where the minimum distance between the molecule and the NbC (111) surface is around 2.20 Å, with an adsorption energy of −0.261 eV.

**CH₃OH.** At an inclination of 77.5° to the surface, this molecule adsorbs above the C atom with an O–C bond length of 1.46 Å and an adsorption energy of −1.614 eV.

**CH₂.** Here, the C atom is attached at the bridging site, at a C–C distance of 1.36 Å to the NbC (111) surface and an adsorption energy of −7.418 eV.

**CH₃.** CH₃ adsorbs to the surface through C–C bonding at 1.49 Å with and adsorption energy of −4.528 eV.

**CH₄.** The long interaction distance of 3.17 Å and small adsorption energy of −0.161 eV indicates physical adsorption of CH₄ at the surface.

The calculated adsorption energies of the intermediates on the C-terminated NbC (111) surface show highly localized, strong interaction between the adsorbates and the surface. All adsorption geometries where the intermediates adsorb on the surface *via* their carbon atoms are energetically preferred over those structures that attach to the surface *via* their oxygen atoms. These results indicate the formation of C–C bonds between the adsorbates and surface, in accord with the large energies released, when these species adsorb on the molybdenum carbide surface *via* attachment to a surface carbon atom.[45]

### 3.2. Reaction networks in the $CO_2$ hydrogenation process

Fig. 2 depicts the reaction pathways that result in the production of the products, *e.g.* CO, HCOOH, $CH_2O$, $CH_3OH$, and $CH_4$, that were considered for this study. Mechanisms *via* HCOO or (*trans,cis*)-COOH intermediates act as the foundation for the overall reaction network. In the next section, the reaction pathways are discussed, using the optimum adsorption geometries for all intermediates.

### 3.3. Chemical reactions

We have studied the possible processes of $CO_2$ hydrogenation over the NbC (111) plane, which are discussed in detail in this section. Table 2 shows the predicted reaction energies for all elementary steps in the hydrogenation at the NbC (111) surface.

Formate, HCOO*, or carboxyl species, *trans*-COOH* (*t*-COOH*) and/or *cis*-COOH* (*c*-COOH*) were formed as a consequence of the initial step of $CO_2$ hydrogenation *via* the reactions:

$$CO_2* + H* \rightarrow HCOO* \qquad (3)$$

$$CO_2* + H* \rightarrow (t,c)\text{-COOH}* \qquad (4)$$

The generation of HCOO* and *c*-COOH* are endothermic processes, with reaction energies of 4.334 and 0.369 eV, respectively, whereas the generation of *t*-COOH* is an exothermic process with an energy of −0.005 eV. Through the HCOO* + H* → HCOOH* reaction, HCOO* can gradually hydrogenate to formic acid (HCOOH), with an exothermic energy of −2.080 eV, whereas the combination of hydrogen atoms with carboxyl species (*c*-COOH* and *t*-COOH*) also forms HCOOH*.
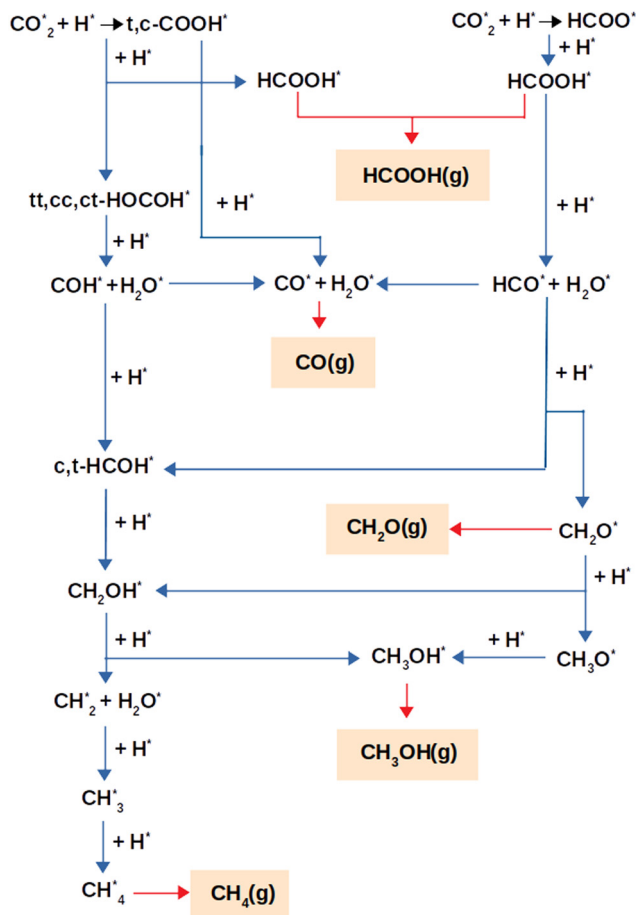
**2502** | *Phys. Chem. Chem. Phys.*, 2023, **25**, 2498–2509

This journal is © the Owner Societies 2023

**Fig. 2** Possible $CO_2$ hydrogenation reaction mechanisms on the NbC (111) surface.

Such processes ($c,t$-COOH* + H* → HCOOH*) are endothermic, with *cis* and *trans* conformers requiring energies of 1.886 eV and 2.259 eV, respectively. Dihydroxycarbenes ($cc$-HOCOH*,

$ct$-HOCOH*, and $tt$-HOCOH*) are formed through the hydrogenation of carboxyl species ($c$-COOH and $t$-COOH) *via* basic reactions of $c,t$-COOH* + H* → (ct, cc, tt)-HOCOH*. The production of $tt$-HOCOH* and $cc$-HOCOH* from $t$-COOH* and $c$-COOH* conformers is an endothermic process, with reaction energies of 0.676 eV and 0.082 eV, respectively. The production of the $ct$-HOCOH* conformer from $t$-COOH* results in the release of a reaction energy of 0.336 eV, whereas the synthesis of the $ct$-HOCOH* conformer from $c$-COOH* releases 0.038 eV of energy. Exothermic reactions of $ct$-HOCOH* → $tt$-HOCOH* and $cc$-HOCOH* → $tt$-HOCOH* with reaction energies of −0.254 and −0.968 eV, respectively, result in the converstion of $ct$-HOCOH and $cc$-HOCOH to $tt$-HOCOH.

This network of reactions results in additional products using two different hydrogenation mechanisms, one through HCOOH* and the other through a HOCOH*. Detailed descriptions of these mechanisms are shown below.

**3.3.1. Product formation through formic acid.** Fig. 3 shows the reaction profiles and associated energy values of several possible routes for the hydrogenation of $CO_2$ and following intermediates to HCOOH, CO, $CH_2O$, $CH_3OH$, and $CH_4$ over the NbC (111) surface. The reaction pathways leading to various products are discussed in further detail in the following sections.

*3.3.1.1. Formic acid formation.* HCOOH may be formed in any one of three ways, as was stated already. Initially, $CO_2$ is hydrogenated to generate HCOO* which subsequently receives another H to produce HCOOH. The other process goes through hydrogenation of $CO_2$ to $t$-COOH* or $c$-COOH* with the production of HCOOH* as an end product of further hydrogenation of $(t,c)$-COOH*. The hydrogenation of $CO_2$ to generate HCOO* requires 4.33 eV, whereas the synthesis of HCOOH from the HCOO* product is an exothermic reaction. Thus, the generation of HCOOH through the $(t,c)$-COOH* intermediate is

**Table 2** Possible elementary steps and their related energies

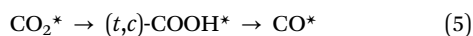| Elementary reactions | $\Delta E$ (eV) | Elementary reactions | $\Delta E$ (eV) |
|---|---|---|---|
| $CO_2$ (g) → $CO_2$* | −0.358 | $c$-COOH* + H* → $cc$-HOCOH* | 0.676 |
| $CO_2$* + H* → HCOO* | 4.334 | $t$-COOH* + H* → $tt$-HOCOH* | 0.082 |
| $CO_2$* + H* → $c$-COOH* | 0.369 | $c$-COOH* + H* → $ct$-HOCOH* | −0.038 |
| $CO_2$* + H* → $t$-COOH* | −0.005 | $t$-COOH* + H* → $ct$-HOCOH* | 0.336 |
| HCOO* + H* → HCOOH* | −2.080 | $cc$-HOCOH* → $tt$-HOCOH* | −0.968 |
| $c$-COOH* + H* → CO* + $H_2O$* | −0.930 | $ct$-HOCOH* → $tt$-HOCOH* | −0.254 |
| $t$-COOH* + H* → CO* + $H_2O$* | -0.556 | $tt$-HOCOH* + H* → COH* + $H_2O$* | 1.205 |
| $c$-COOH* + H* → HCOOH* | 1.886 | $ct$-HOCOH* + H* → COH* + $H_2O$* | 0.951 |
| $t$-COOH* + H* → HCOOH* | 2.259 | $cc$-HOCOH* + H* → COH* + $H_2O$* | 0.237 |
| HCOOH* → HCO* + $H_2O$* | 0.234 | COH* → CO* + H* | −1.843 |
| HCOOH* → HCOO (g) | 1.539 | COH* + H* → $t$-HCOH* | 1.116 |
| HCO* + H* → $t$-HCOH* | −0.090 | COH* + H* → $c$-HCOH* | 1.429 |
| HCO* + H* → $c$-HCOH* | 0.223 | $t$-HCOH* + H* → $CH_2OH$* | 2.711 |
| HCO* → CO* + H* | −3.049 | $c$-HCOH* + H* → $CH_2OH$* | 2.398 |
| CO* → CO (g) | 4.008 | $CH_2OH$* + H* → $CH_2$* + $H_2O$* | −0.357 |
| HCO* + H* → $CH_2O$* | 2.068 | $CH_2$* + H* → $CH_3$* | 1.830 |
| $CH_2O$* → $CH_2O$ (g) | 1.908 | $CH_3$* + H* → $CH_4$* | 3.105 |
| $CH_2O$* + H* → $CH_3O$* | 4.857 | $CH_4$* → $CH_4$(g) | 0.161 |
| $CH_2O$* + H* → $CH_2OH$* | 0.553 | $CH_3OH$* → $CH_3OH$ (g) | 1.641 |
| $CH_3O$* + H* → $CH_3OH$* | −2.338 | $H_2O$* → $H_2O$ (g) | 1.226 |
| $CH_2OH$* + H* → $CH_3OH$* | 1.967 | | |
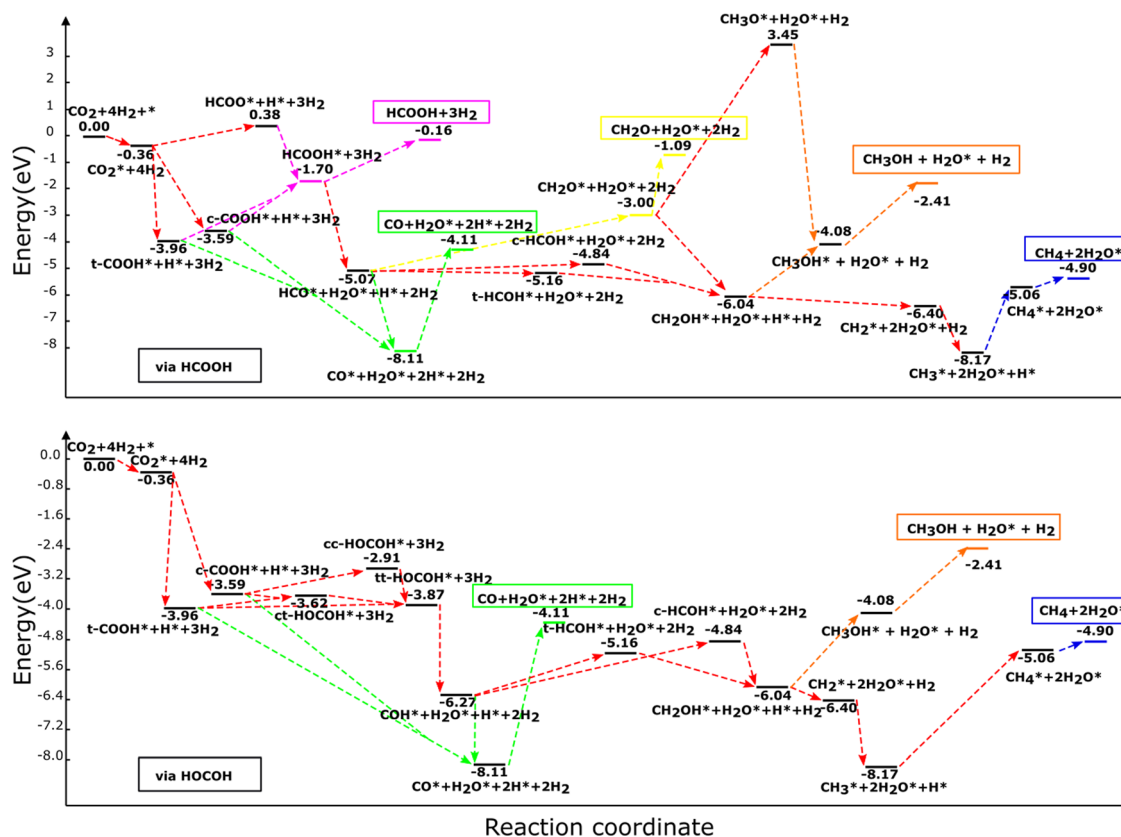
**Fig. 3** Reaction profile for the hydrogenation of $CO_2$ and all intermediates to HCOOH, CO, $CH_2O$, $CH_3OH$, and $CH_4$ molecules *via* (a) HCOOH and (b) HOCOH on the NbC (111) plane. The illustrated profiles are associated with the total free energy of the catalyst, $CO_2$, and four $H_2$ molecules in the gas phase.[46]

thermodynamically more advantageous than the HCOO* pathway (see Table 2).

*3.3.1.2 Carbon monoxide formation via formic acid.* The (*t,c*)-COOH* and the HCOOH* pathways are the two main routes by which carbon monoxide is produced. In the first, CO is formed through the degradation of (*t,c*)-COOH* using the chemical mechanism of (*t,c*)-COOH* + H* → CO* + $H_2$O*, which are exothermic processes with reaction energies of −0.556 and −0.930 eV, for the *trans* and *cis* conformers, respectively.

Breakdown of HCOOH* to HCO* (HCOOH* + H* → HCO* + $H_2$O*) leads to an endothermic reaction energy of 0.234 eV, which is followed by HCO* dehydrogenation (HCO* → CO* + H*) to produce CO with a reaction energy of −3.049 eV. In consequence, the general reactions for CO production using HCOOH may be written as:

$$CO_2^* \rightarrow (t,c)\text{-}COOH^* \rightarrow CO^* \quad (5)$$

$$CO_2^* \rightarrow t\text{-}COOH^* \rightarrow HCOOH^* \rightarrow HCO^* \rightarrow CO^* \quad (6)$$

*3.3.1.3 Formaldehyde formation via formic acid.* The sole pathway to obtain $CH_2O$ from $CO_2$ is *via* HCO*, where HCO* accepts hydrogen to generate $CH_2O$. Formaldehyde ($CH_2O$*) or (*c,t*)-HCOH* may be formed *via* the hydrogenation of HCO*,

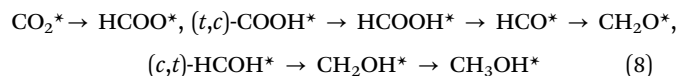with an endothermic energy of 2.068 eV for HCO* + H* → $CH_2O$*. As a result, the following are the main reactions involved in producing $CH_2O$:

$$CO_2^* \rightarrow HCOO^*, (t,c)\text{-}COOH^* \rightarrow HCOOH^* \rightarrow HCO^* \rightarrow CH_2O^* \quad (7)$$
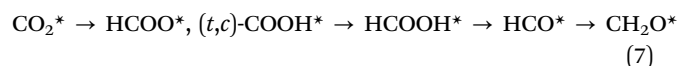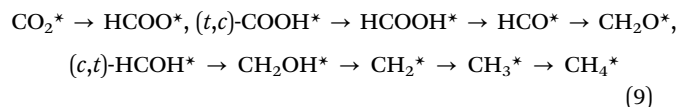
*3.3.1.4. Methanol formation via formic acid.* It has been suggested previously that with reaction energies of 0.223 eV and −0.090 eV, respectively, for the *cis* and *trans* conformers, hydrogenation of HCO* may result in the creation of (*c,t*)-HCOH* through the reaction HCO* + H* → (*c,t*)-HCOH*. HCO* hydrogenation should therefore generate the *t*-HCOH* conformer more often, since it is an exothermic reaction.

Additional hydrogenation of (*c,t*)-HCOH* or $CH_2O$* may lead to the formation of $CH_3OH$. *t*-HCOH* and $CH_2O$* are hydrogenated, but the former occurs through the *t*-HCOH* + H* → $CH_2OH$* mechanism, whereas the latter is achieved through $CH_2O$* *via* $CH_2O$* + H* → $CH_2OH$*. In order to produce $CH_2OH$*, a total of 2.711 eV and 0.553 eV of energy is required for the two separate processes. $CH_2OH$* is more likely to be generated *via* $CH_2O$* hydrogenation than through *t*-HCOH*, because the hydrogenation of $CH_2O$* to $CH_2OH$* is more efficient in terms of energy than the hydrogenation of

**2504** | *Phys. Chem. Chem. Phys.*, 2023, **25**, 2498–2509

This journal is © the Owner Societies 2023

*t*-HCOH*. Continuing the hydrogenation of CH$_2$OH* results in the formation of CH$_3$OH* (CH$_2$OH* + H* → CH$_3$OH*), distinguished by its endothermic nature with an energy of 1.967 eV. Hydrogenation of CH$_2$O* may also produce methoxy (CH$_3$O*), in addition to CH$_2$OH*. However, whereas this mechanism happens *via* CH$_2$O* + H* → CH$_3$O* and consumes a significant amount of energy (4.857 eV), the following hydrogenation stage leads to CH$_3$OH* *via* CH$_3$O* + H* → CH$_3$OH* which releases just 2.338 eV of reaction energy. Although it is energetically possible to produce CH$_3$OH using CH$_3$O, the recommended method is to go through CH$_2$OH* hydrogenation to produce CH$_3$OH* owing to the less endothermic reaction involved. For CH$_3$OH* synthesis, the suggested sequence of steps is as follows:
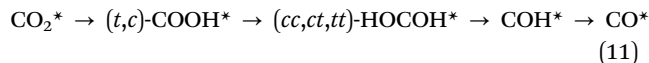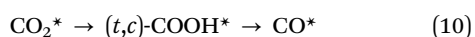
$$CO_2^* \rightarrow HCOO^*, (t,c)\text{-}COOH^* \rightarrow HCOOH^* \rightarrow HCO^* \rightarrow CH_2O^*,$$
$$(c,t)\text{-}HCOH^* \rightarrow CH_2OH^* \rightarrow CH_3OH^* \qquad (8)$$

*3.3.1.5. Methane formation via formic acid.* Only dissociation of CH$_2$OH* (CH$_2$OH* + H* → CH$_2$* + H$_2$O*) results in the synthesis of CH$_2$*, and the end products CH$_3$* and CH$_4$*. Reactions CH$_2$* + H* → CH$_3$ and CH$_3$* + H* → CH$_4$* may generate CH$_4$* by hydrogenating CH$_2$* and CH$_3$* with reaction energies of 1.830 eV and 3.105 eV for the production of CH$_3$* and CH$_4$*, respectively. The following is an ordinary sequence, indicating some reactions that contribute to the synthesis of CH$_4$* from HCOOH*:
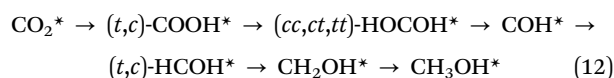
$$CO_2^* \rightarrow HCOO^*, (t,c)\text{-}COOH^* \rightarrow HCOOH^* \rightarrow HCO^* \rightarrow CH_2O^*,$$
$$(c,t)\text{-}HCOH^* \rightarrow CH_2OH^* \rightarrow CH_2^* \rightarrow CH_3^* \rightarrow CH_4^* \qquad (9)$$

**3.3.2. Product formation *via* dihydroxycarbene.** It has already been mentioned that the hydrogenation of (*t,c*)-COOH* may generate CO, CH$_3$OH, and CH$_4$. As a result of the exothermic nature of the transformation of *cc*-HOCOH* and *ct*-HOCOH* to *tt*-HOCOH* ((*cc,ct*)-HOCOH* + H* → *tt*-HOCOH*), with respective energies of −0.968 eV and −0.254 eV, the *tt*-HOCOH* species is likely to be dominant on the surface.
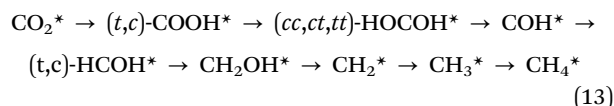
*3.3.2.1. Carbon monoxide formation via dihydroxycarbene.* From the direct breakdown of (*t,c*)-COOH*, CO* may be produced, although it can also be produced *via* COH*. The first route was described in detail in Section 3.3.1.2, where the processes were found to be exothermic with energies of −0.556 eV *via* the *cis* and −0.930 eV *via* the *trans* conformer. In the second route, COH* and H$_2$O* are formed *via* the breakdown of the most suitable HOCOH* conformers (*tt*-HOCOH*) *via* the reaction *tt*-HOCOH* + H* → COH* + H$_2$O* with a reaction energy of 1.205 eV. Further breakdown of COH* (COH* → CO* + H*) leads to the generation of CO*. CO* tends to be created through the COH* route with the exothermic mechanism of creating CO* from COH* with a reaction energy of −1.843 eV. As a consequence, the reactions for CO production using HOCOH* could be written as:

$$CO_2^* \rightarrow (t,c)\text{-}COOH^* \rightarrow CO^* \qquad (10)$$

$$CO_2^* \rightarrow (t,c)\text{-}COOH^* \rightarrow (cc,ct,tt)\text{-}HOCOH^* \rightarrow COH^* \rightarrow CO^* \qquad (11)$$

*3.3.2.2. Methanol production from dihydroxycarbene.* Trans-HCOH* or *cis*-HCOH* is formed after addition of a hydrogen atom *via* COH* + H* → *t*-HCOH* and COH* + H* → *c*-HCOH* with endothermic energies of 1.116 eV and 1.429 eV, respectively. Further hydrogenation of (*t,c*)-HCOH* results in the formation of CH$_2$OH* *via* the process (*t,c*)-HCOH* + H* → CH$_2$OH*. CH$_3$OH* is then generated through additional hydrogenation of CH$_2$OH*. The creation of CH$_2$OH* from (*t,c*)-HCOH* and the generation of CH$_3$OH* from CH$_2$OH* are endothermic processes with reaction energies of 2.711 eV, 2.398 eV and 1.967 eV. Based on the relative energies, we suggest that the following route is the most likely to lead to the generation of CH$_3$OH*:

$$CO_2^* \rightarrow (t,c)\text{-}COOH^* \rightarrow (cc,ct,tt)\text{-}HOCOH^* \rightarrow COH^* \rightarrow$$
$$(t,c)\text{-}HCOH^* \rightarrow CH_2OH^* \rightarrow CH_3OH^* \qquad (12)$$

*3.3.2.3. Methane formation via dihydroxycarbene.* Decomposition of CH$_2$OH* into either HOCOH or HCOOH results in the production of CH$_2$* and its further hydrogenation. As a result, the following route is suggested to generate CH$_4$* *via* HOCOH*:

$$CO_2^* \rightarrow (t,c)\text{-}COOH^* \rightarrow (cc,ct,tt)\text{-}HOCOH^* \rightarrow COH^* \rightarrow$$
$$(t,c)\text{-}HCOH^* \rightarrow CH_2OH^* \rightarrow CH_2^* \rightarrow CH_3^* \rightarrow CH_4^* \qquad (13)$$

**3.4. Electronic properties from CO$_2$ adsorption**

Charge densities and total densities of state (TDOS) are calculated to gain more detailed insight into the CO$_2$ adsorption at the NbC (111) surface. The density of states is large around the Fermi level, as seen in Fig. 4a, and there is no energy gap at this level. A partly filled d band and potentially occupied s orbital in NbC may contribute to the metal characteristics of the compound, which is consistent with previous observations.[3,4] The TDOS behaves in a manner comparable to the behavior of the DOS of the Nb atoms, and both above and below the Fermi level, the participation of Nb atoms in the TDOS is much greater than that of the C atoms, because the electronic structure of NbC is defined by surface states formed of Nb 4d orbitals at about $E_F$.[47,48] However, Fig. 4b demonstrates that whenever a CO$_2$ molecule is adsorbed on the NbC (111) surface, there is no substantial variation in the TDOS, apart from a slight increase at the Fermi level.

Next, we have used equation (2) to determine the charge density difference caused by CO$_2$ adsorption by considering separately the charge density of CO$_2$ + NbC (111), the bare slab, and the isolated CO$_2$. Fig. 4c depicts the rearrangement of charge density in the system following CO$_2$ adsorption, where yellow indicates a positive charge difference and blue indicates a negative charge difference. CO$_2$ is seen to have accumulated

This journal is © the Owner Societies 2023

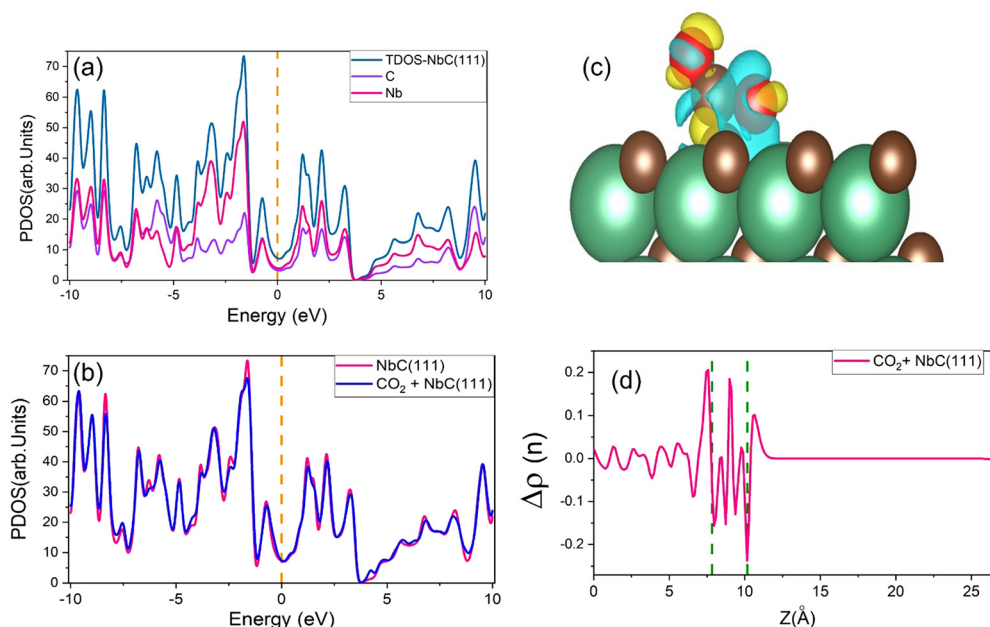*Phys. Chem. Chem. Phys.*, 2023, **25**, 2498–2509 | **2505**

Fig. 4 (a) The PDOS for the NbC (111) surface, (b) the TDOS of NbC (111) prior to and after adsorption of $CO_2$, (c) view of the charge density differences, with the C and O atoms illustrated in brown and red (isovalue = ±0.002) and, (d) the planar average charge density. The Fermi level is set at zero.

negative charge upon adsorption at the surface. We have also used the planar mean charge density differential $\Delta\rho(z)^{23}$ to investigate the charge rearrangement of $CO_2$ following adsorption on NbC (111), as shown below:

$$\Delta\rho(z) = \Delta\rho(z)_{\text{Molecule+NbC(111)}} - \Delta\rho(z)_{\text{NbC(111)}} - \Delta\rho(z)_{\text{Molecule}} \tag{14}$$

where $\Delta\rho(z)_{\text{Molecule+NbC(111)}}$, $\Delta\rho(z)_{\text{NbC(111)}}$, and $\Delta\rho(z)_{\text{Molecule}}$ represent the planar mean charge densities of the relaxed Molecule + NbC(111) system, bare NbC (111) slab, and the isolated $CO_2$ molecule, respectively. The dashed zone in Fig. 4d represents the site of $CO_2$ on the NbC (111) surface. The negative (positive) values of $\Delta\rho(z)$ zones indicate the charge density increase (depletion) sites following the adsorption of $CO_2$.

**3.4.1 Electronic properties of the products.** TDOS and charge densities for $CH_4$, CO, $CH_2O$, and $CH_3OH$ products are shown in Fig. 5 to better explain the desorption mechanism. Whether present or absent from the surface, the TDOS for $CH_4$ and CO adopt a similar pattern, as seen in Fig. 5a and b, particularly near the Fermi level. As seen in Fig. 5c and d, the TDOS for $CH_3OH$ and $CH_2O$ shift somewhat towards positive energies and diverge from the NbC (111) TDOS when the adsorbates are present. From the data presented here, it can be concluded that modest variations in charge transmission happen throughout the adsorption process. Given the nature of their bonding to the surface, the TDOS of the adsorption arrangements for $CH_3OH$ and $CH_2O$ deviate further from the TDOS of the bare slab than those for $CH_4$ and CO. In contrast to the $CH_4$ and CO molecules adsorbing on the surface using their carbon atoms, the $CH_3OH$ and $CH_2O$ compounds connect to the surface using their oxygen atoms, causing the NbC (111)

TDOS to deviate by a small amount from those of the bare surface.

## 4. Conclusion

In this investigation, we have calculated the energetics of the interaction of 25 reactant, intermediate and product species at the carbon-terminated NbC (111) surface and we have evaluated their reactions in the $CO_2$ hydrogenation process, where it has been shown that methane has the maximum capacity for hydrogen of all the investigated products.

$CH_2O$ generation is expected to be produced predominantly from HCOOH rather than other intermediates, because the endothermic reaction energies for the production of $CH_4$, $CH_3OH$ and CO *via* HCOOH are rather high, and the route through HCOOH is thus not practical for the synthesis of $CH_3OH$, $CH_4$ or CO. The suggested pathways for each product have been collected in Fig. 6 to allow direct comparison. According to our findings, 4.902 eV in energy is generated during $CO_2$ hydrogenation to methane over the C-terminated NbC (111) surface through the route:
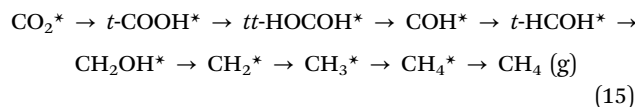
$$CO_2^* \rightarrow t\text{-COOH}^* \rightarrow tt\text{-HOCOH}^* \rightarrow COH^* \rightarrow t\text{-HCOH}^* \rightarrow$$
$$CH_2OH^* \rightarrow CH_2^* \rightarrow CH_3^* \rightarrow CH_4^* \rightarrow CH_4 \text{ (g)} \tag{15}$$

Fig. 6a shows the desorption of $CH_4$ into the gas phase as a result of this reaction. The second strongly exothermic $CO_2$ hydrogenation mechanism, releasing an energy of 4.107 eV, is the route to CO generation (Fig. 6b):
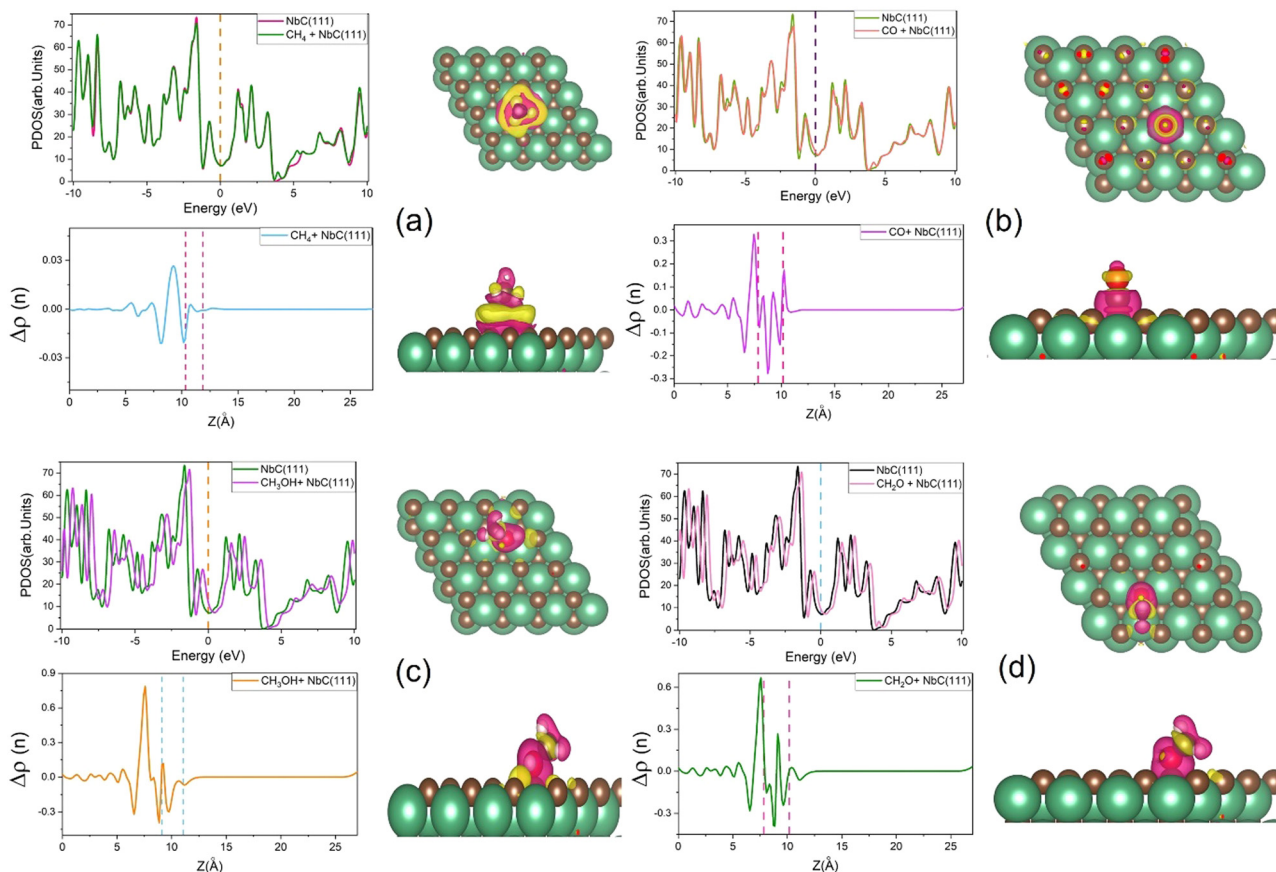
$$CO_2^* \rightarrow t\text{-COOH}^* \rightarrow tt\text{-HOCOH}^* \rightarrow COH^* \rightarrow CO^* \rightarrow CO \text{ (g)} \tag{16}$$

**2506** | *Phys. Chem. Chem. Phys.*, 2023, **25**, 2498–2509

This journal is © the Owner Societies 2023

**Fig. 5** The TDOS, the planar average charge densities, and charge density differences for (a) $CH_4$ (isovalue = $\pm 0.00005$), (b) CO (isovalue = $\pm 0.001$), (c) $CH_3OH$ (isovalue = $\pm 0.002$) and, (d) $CH_2O$ (isovalue = $\pm 0.002$). The Fermi level is set at zero.
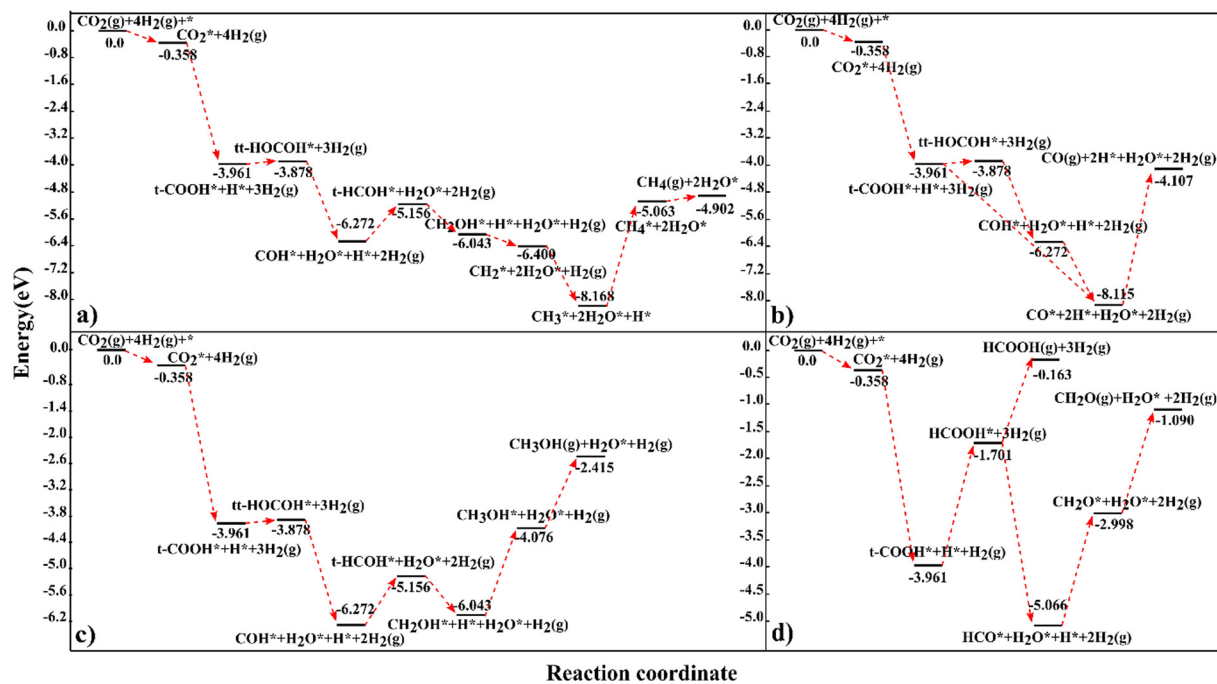


**Fig. 6** The preferred reaction profiles for $CO_2$ hydrogenation to (a) $CH_4$, (b) CO, (c) $CH_3OH$, and (d) $CH_2O$ and HCOOH on the NbC (111) plane. The illustrated profiles are compared to the summation the total free energies of the catalyst, $CO_2$, and four $H_2$ in the gas phase.[46]

This journal is © the Owner Societies 2023

*Phys. Chem. Chem. Phys.*, 2023, **25**, 2498–2509 | **2507**

and

$$CO_2* \rightarrow t\text{-}COOH* \rightarrow CO* \rightarrow CO\ (g) \qquad (17)$$

The obtained results are in agreement with experiments, which have suggested that $CH_4$ and CO are the main products of $CO_2$ hydrogenation over transition metal carbides.[15,45]

$CH_3OH$ is the third possible product with an exothermic energy of 2.415 eV, through the preferred route (Fig. 6c):
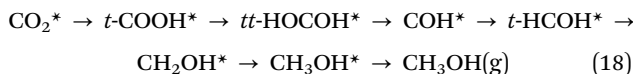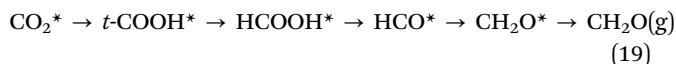
$$CO_2* \rightarrow t\text{-}COOH* \rightarrow tt\text{-}HOCOH* \rightarrow COH* \rightarrow t\text{-}HCOH* \rightarrow$$
$$CH_2OH* \rightarrow CH_3OH* \rightarrow CH_3OH(g) \qquad (18)$$

Fig. 6d shows that $CH_2O$ and HCOOH production, releasing energies of 1.090 and 0.163 eV, respectively, are the least likely products of $CO_2$ hydrogenation based on the routes:

$$CO_2* \rightarrow t\text{-}COOH* \rightarrow HCOOH* \rightarrow HCO* \rightarrow CH_2O* \rightarrow CH_2O(g) \qquad (19)$$

and

$$CO_2* \rightarrow t\text{-}COOH* \rightarrow HCOOH* \rightarrow HCOOH\ (g) \qquad (20)$$

In conclusion, we have used DFT calculations to investigate a comprehensive network of reaction pathways for $CO_2$ hydrogenation to $CH_4$, CO, $CH_3OH$, $CH_2O$ and HCOOH over the carbon-terminated NbC (111) surface. By evaluating the predicted reaction energies, we can conclude that the most abundant products should be $CH_4$ and CO, followed to a lesser extent by $CH_3OH$, $CH_2O$, and HCOOH, which findings are in excellent agreement with experimental findings.

The calculated adsorption energies of the intermediates on the surface show highly localized strong interactions between the adsorbates and the surface, which lead to an overall exothermic reaction pathway that provides sufficient energy to overcome the desorption energy required to release the products from the surface. Furthermore, where there is co-adsorption of the hydrogen and the intermediates at the surface, the hydrogenation step energies indicate that the presence of hydrogen on the surface makes the intermediates more reactive, which as a result readily undergo further surface-mediated reactions to form $CH_4$, CO and the other products.

The carbon-terminated (111) surfaces of TMCs are generally less stable than the metal-terminated planes. However, Quesne *et al.*[5] calculated the energies of both carbon- and metal-terminated surfaces across the TMC series, where the carbon-terminated (111) surfaces of NbC, TaC, MoC and WC were found to be preferred over the metal-terminated surfaces. The carbon-terminated NbC (111) was also found to be important in a number of other studies,[5,7,20,34] whereas our results also indicate that the carbon-terminated NbC (111) surface remains stable during the adsorption of $CO_2$. Furthermore, the results from this study indicate that $CO_2$ adsorption on the carbon-terminated NbC (111) surface at $E_{ads} = -0.358$ eV is weaker than at the metal-terminated NbC (111) with $E_{ads} = -1.863$ eV (calculated in our previous study[32]). We have also found a larger exothermic reaction energy for $CO_2$ methanation on the carbon-terminated surface, releasing 4.902 eV, than the

same process at the metal-terminated surface, releasing 2.747 eV, as calculated in our previous work.[32] Overall, the results suggest that the carbon-terminated surface should be a promising catalyst for $CO_2$ hydrogenation, allowing an energetically favourable hydrogenation process.

From our calculations, we can make a number of secondary observations. For example, it is much more advantageous to produce CO immediately from either $t$-COOH or COH* degradation through the $tt$-HOCOH route. Furthermore, the majority of $CH_4$, CO, and $CH_3OH$ is generated by $t$-COOH* *via* the $tt$-HOCOH route, whereas the majority of $CH_2O$ originates from HCO* *via* the HCOOH reaction. Along these routes, HCO* fragmentation has the highest exothermic reaction energy of $-3.049$ eV, whereas $CH_3$* hydrogenation to $CH_4$* requires the highest endothermic reaction energy of 3.105 eV.

It is worth mentioning that in this study we have only investigated the thermodynamics of the reactions, without considering the kinetics and activation energies. The proposed mechanisms were suggested based on the comparative reaction energies of the different pathways, which identified the energetically favoured reaction mechanism. The inclusion of transition states in the catalytic pathways would provide further insight, for example allowing us to identify the rate-determining step, but it would not invalidate the thermodynamically favourable reaction pathway.

We have also assessed the electronic features of the system of $CO_2$ and the intermediates formed as a result of its hydrogenation over the C-terminated NbC (111) surface, which have indicated that the adsorbates have little effect on the surface.

This work has led to detailed understanding of some of the fundamental steps in the $CO_2$ catalytic hydrogenation mechanism at the C-terminated NbC (111) surface which results in the production of C1 type surface species. Since the field of $CO_2$ hydrogenation still requires significant advances in the understanding of reaction mechanisms for C–C coupling, for synthesis of higher alcohols and higher hydrocarbons, further potential pathways leading to the production of other useful compounds have yet to be explored. However, we consider that the results of this work may assist experiment in the development of effective catalysts based on transition metal carbides.

## Data availability statement

The data that support the findings of this study are available on request from the corresponding author.

## Conflicts of interest

There are no competing interest to declare.

## Acknowledgements

**2508** | *Phys. Chem. Chem. Phys.*, 2023, **25**, 2498–2509

This journal is © the Owner Societies 2023

# References

1 B. I. Sharma, J. Maibam, R. Paul, R. Thapa and R. B. Singh, *Indian J. Phys.*, 2010, **84**, 671–674.

2 J. A. Rodriguez, J. Evans, L. Feria, A. B. Vidal, P. Liu, K. Nakamura and F. Illas, *J. Catal.*, 2013, **307**, 162–169.

3 F. Viñes, C. Sousa, P. Liu, J. Rodriguez and F. Illas, *J. Chem. Phys.*, 2005, **122**, 174709.

4 K. Kobayashi, *Jpn. J. Appl. Phys.*, 2000, **39**, 4311.

5 M. G. Quesne, A. Roldan, N. H. de Leeuw and C. R. A. Catlow, *Phys. Chem. Chem. Phys.*, 2018, **20**, 6905–6916.

6 H. W. Hugosson, O. Eriksson, U. Jansson and B. Johansson, *Phys. Rev. B: Condens. Matter Mater. Phys.*, 2001, **63**, 134108.

7 H. H. Hwu and J. G. Chen, *Chem. Rev.*, 2005, **105**, 185–212.

8 A. Vojvodic, C. Ruberto and B. I. Lundqvist, *J. Phys.: Condens. Matter*, 2010, **22**, 375504.

9 F. Viñes, J. A. Rodriguez, P. Liu and F. Illas, *J. Catal.*, 2008, **260**, 103–112.

10 P. Liu and J. A. Rodriguez, *J. Phys. Chem. B*, 2006, **110**, 19418–19425.

11 N. M. Schweitzer, J. A. Schaidle, O. K. Ezekoye, X. Pan, S. Linic and L. T. Thompson, *J. Am. Chem. Soc.*, 2011, **133**, 2378–2381.

12 P. M. Patterson, T. K. Das and B. H. Davis, *Appl. Catal., A*, 2003, **251**, 449–455.

13 C. Kunkel, F. Vines and F. Illas, *Energy Environ. Sci.*, 2016, **9**, 141–144.

14 S. Posada-Pérez, F. Vines, P. J. Ramirez, A. B. Vidal, J. A. Rodriguez and F. Illas, *Phys. Chem. Chem. Phys.*, 2014, **16**, 14912–14921.

15 M. D. Porosoff, S. Kattel, W. Li, P. Liu and J. G. Chen, *Chem. Commun.*, 2015, **51**, 6988–6991.

16 S. Posada-Pérez, F. Viñes, P. J. Ramirez, A. B. Vidal, J. A. Rodriguez and F. Illas, *Phys. Chem. Chem. Phys.*, 2014, **16**, 14912–14921.

17 M. D. Porosoff, X. Yang, J. A. Boscoboinik and J. G. Chen, *Angew. Chem.*, 2014, **126**, 6823–6827.

18 Q. Zhang, L. Pastor-Pérez, W. Jin, S. Gu and T. R. Reina, *Appl. Catal., B*, 2019, **244**, 889–898.

19 S. Posada-Pérez, P. J. Ramírez, R. A. Gutiérrez, D. J. Stacchiola, F. Viñes, P. Liu, F. Illas and J. A. Rodriguez, *Catal. Sci. Technol.*, 2016, **6**, 6766–6777.

20 M. G. Quesne, A. Roldan, N. H. de Leeuw and C. R. A. Catlow, *Phys. Chem. Chem. Phys.*, 2019, **21**, 10750–10760.

21 Z. Ou, C. Qin, J. Niu, L. Zhang and J. Ran, *Int. J. Hydrogen Energy*, 2019, **44**, 819–834.

22 S. Posada-Pérez, P. J. Ramírez, J. Evans, F. Viñes, P. Liu, F. Illas and J. A. Rodriguez, *J. Am. Chem. Soc.*, 2016, **138**, 8269–8278.

23 N. Y. Dzade and N. H. d Leeuw, *Catalysts*, 2021, **11**, 127.

24 S. S. Tafreshi, A. Z. Moshfegh and N. H. de Leeuw, *J. Phys. Chem. C*, 2019, **123**, 22191–22201.

25 X. Liu, C. Kunkel, P. Ramírez de la Piscina, N. Homs, F. Viñes and F. Illas, *ACS Catal.*, 2017, **7**, 4323–4335.

26 K. Edamoto, E. Shiobara, T. Anazawa, M. Hatta, E. Miyazaki, H. Kato and S. Otani, *J. Chem. Phys.*, 1992, **96**, 842–847.

27 K. Edamoto, E. Miyazaki and H. Kato, *Vacuum*, 1990, **41**, 547–549.

28 S. Tokumitsu, T. Anazawa, O. Ozawa, R. Sekine, E. Miyazaki, K. Edamoto, H. Kato and S. Otani, *Phys. Rev. B: Condens. Matter Mater. Phys.*, 1995, **51**, 4516.

29 K. Edamoto, Y. Abe, T. Ikeda, N. Ito, E. Miyazaki, H. Kato and S. Otani, *Surf. Sci.*, 1990, **237**, 241–247.

30 K. Edamoto, S. Maehama, E. Miyazaki and H. Kato, *Phys. Rev. B: Condens. Matter Mater. Phys.*, 1989, **39**, 7461–7465.

31 K. Ozawa, S. Ishikawa, E. Miyazaki, K. Edamoto, H. Kato and S. Otani, *Surf. Sci.*, 1997, **375**, 250–256.

32 S. Sarabadani Tafreshi, M. Ranjbar, N. Taghizade, S. F. K. S. Panahi, M. Jamaati and N. H. de Leeuw, *ChemPhysChem*, 2022, **23**, e202100781.

33 K. E. Tan, M. W. Finnis, A. P. Horsfield and A. P. Sutton, *Surf. Sci.*, 1996, **348**, 49–54.

34 F. Silveri, M. G. Quesne, A. Roldan, N. H. De Leeuw and C. R. A. Catlow, *Phys. Chem. Chem. Phys.*, 2019, **21**, 5335–5343.

35 A. S. Botana and M. R. Norman, *Phys. Rev. Mater.*, 2019, **3**, 044001.

36 G. Kresse and J. Furthmüller, *Comput. Mater. Sci.*, 1996, **6**, 15–50.

37 J. Perdew, K. Burke and M. Ernzerhof, *Phys. Rev. Lett.*, 1998, **80**, 891.

38 G. Kresse and J. Hafner, *J. Phys.: Condens. Matter*, 1994, **6**, 8245.

39 P. E. Blöchl, *Phys. Rev. B: Condens. Matter Mater. Phys.*, 1994, **50**, 17953–17979.

40 S. Grimme, S. Ehrlich and L. Goerigk, *J. Comput. Chem.*, 2011, **32**, 1456–1465.

41 H. J. Monkhorst and J. D. Pack, *Phys. Rev. B: Condens. Matter Mater. Phys.*, 1976, **13**, 5188–5192.

42 S. S. Tafreshi, A. Roldan and N. H. de Leeuw, *Phys. Chem. Chem. Phys.*, 2015, **17**, 21533–21546.

43 S. Sarabadani Tafreshi, S. F. K. S. Panahi, N. Taghizade, M. Jamaati, M. Ranjbar and N. H. de Leeuw, *Catalysts*, 2022, **12**, 1275.

44 https://icsd.products.fiz-karlsruhe.de.

45 K.-Z. Qi, G.-C. Wang and W.-J. Zheng, *Surf. Sci.*, 2013, **614**, 53–63.

46 R. A. Angnes, mechaSVG, GitHub repository, 2020, DOI: 10.5281/zenodo.3970267.

47 K. Ozawa, S. Ishikawa, S. Tokumitsu, R. Sekine, E. Miyazaki, K. Edamoto, H. Kato and S. Otani, *Surf. Sci.*, 1996, **364**, L612–L616.

48 K. Ozawa, S. Ishikawa, K. Edamoto, H. Kato and S. Otani, *Surf. Sci.*, 1999, **419**, 226–235.

This journal is © the Owner Societies 2023

*Phys. Chem. Chem. Phys.*, 2023, **25**, 2498–2509 | **2509**